Journal of Air Pollution and Health (Summer 2023); 8(3): 339-360

Original Article

Available online at http://japh.tums.ac.ir

Impact of roof shape on indoor gaseous pollutant level for natural ventilation buildings in a street canyon: Numerical simulation

Haiying Xie, Tianxiao Zhang*

Department of Environmental Science and Engineering, University of Shanghai for Science and Technology, Shanghai, People's Republic of China

ARTICLE INFORMATION

Article Chronology:
Received 21 July 2023
Revised 19 August 2023
Accepted 03 September 2023
Published 29 September 2023

Keywords:
Roof shape; Street canyon; Natural ventilation; Indoor air quality; Numerical simulation

CORRESPONDING AUTHOR:

xiehy@usst.edu.cn
Tel: (+86) 2155271991
Fax: (+86) 55271991

ABSTRACT

Introduction: Coupling the indoor and outdoor airflow of roadside buildings in a street canyon, the impact of flat and triangular roofs on indoor air pollutant concentration and ventilation rates of naturally ventilated buildings is studied using numerical simulation methods.

Materials and methods: The flow and pollutant diffusion control equations are solved by using ANSYS Fluent. In simulation, RNG *k-ε* turbulence model is adopted. The numerical model is validated using the three-dimensional street canyon test data from the wind tunnel experiment at University of Karlsruhe.

Results: The flow and pollutant concentration distributions under different roof shapes are obtained. The ventilation rates with different air flow resistances and pollution level indoors are provided.

Conclusion: Ventilation direction through windows of roadside buildings determines the level of indoor air polluted by vehicle emissions in street canyon. When the building main height equals to the width of the street, flat roofs make the indoor concentration basically consistent with that near the external walls of the canyon. The higher the triangular roofs, the higher the ventilation rate and the lower the indoor concentration. The ventilation rate is influenced not only by roofs, but also by the floor location and indoor ventilation resistance.

Introduction

Due to zero carbon emission, simplicity and comfort, natural ventilation has always been people's first choice to improve indoor air quality when the outdoor air temperature is suitable [1-2]. With the rapid urbanization, however, this traditional ventilation method encounters a challenge. Firstly, the air outdoors is inevitably polluted by vehicle emissions, which is now one of the key pollution sources in urban areas [3-4]. the total emission of gaseous (CO, HC, and NOx) and Particulate Pollutants ($PM_{2.5}$) generated by motor vehicles was more than 40×10^6 t/yr from 2012 to 2018 in China [5]. These pollutants can be transmitted and diffused into the building

Please cite this article as: Xie H, Zhang T. Impact of roof shape on indoor gaseous pollutant level for natural ventilation buildings in a street canyon: Numerical simulation. Journal of Air Pollution and Health. 2023;8(3): 339-360.

through natural ventilation [6-9]. In some unfavorable situations, natural ventilation instead leads to a deterioration of air quality indoors [10, 11]. Secondly, in order to accommodate more than half of the global population who lives in cities [12], urban buildings has to be taller and denser, resulting in the air flow around buildings more complex and also affecting the natural ventilation of buildings [4]. Hence in densely arranged complex, the accurate evaluation of natural ventilation indoors requires coupling the air flow inside and outside of buildings. In addition, it is necessary to simultaneously study the transmission patterns of air pollutants from outdoor to indoor environment in order to propose effective measures for better indoor air quality.

The research methods used in building ventilation mainly includes wind tunnel experiment, field measurement and numerical simulation. In wind tunnel experiments, building scale models are chosen and the studies usually focus on the principle and mechanism of ventilation by measuring the flow near openings [13-15]. By measuring the wind speed and concentration inside and outside of the building model in the wind tunnel, it was found that the presence of other buildings around would cause the air velocity at the opening to be 70% lower than that without the buildings around [13]. For better understanding and evaluating the natural ventilation in real conditions, the impact of fluctuating wind direction on cross-ventilation was investigated using wind tunnel experiment [15]. Due to the fact that the cross-sectional dimensions of wind tunnels are mostly 1-2 m and there is at least one order of magnitude difference between the scales of the building and ventilation openings, it is difficult to perform natural ventilation experiment of building complex in wind tunnels.

Field measurements could provide the most reliable results in real environment without the requirement of similarity criteria in wind tunnel experiment. The disadvantages of the method are time-consuming and difficult to analyze data for the uncontrollable incoming flow including the wind speed, direction and frequency. Moreover, the conclusions obtained from certain studies are not universal due to the diversity of on-site conditions [16]. Under unsteady natural wind conditions, a study took a year to obtain the wind pressure and speed of the full-scale building model [17]. A 9-month research was conducted on the impact of the array on the relationship between local and reference wind speeds and cross ventilation rate [18]. The paper emphasizes the importance of addressing the effects of surrounding buildings on ventilation rate.

The numerical simulation uses Computational Fluid Dynamics (CFD) to achieve the full and detailed flow fields, thus obtaining the ventilation evaluation. The method has gained an increasing popularity for its low cost, saving time, and the ability to simulate flow problems at multiple scales only if computing resources permit [6-8, 19-21]. These simulation studies include single-sided [6, 20] and cross ventilation [7, 8, 19, 21]. As for the driving force, most studies consider the wind-induced ventilation [7, 8, 19-21]. Some investigation considers both wind and buoyancy effects [6]. The isolated building is chosen if the study focuses on ventilation mechanism [6, 19, 20], while street canyons or building complex should be more consistent with actual ventilation conditions when surrounding buildings included [7, 8, 21]. In simulations, using Reynolds-averaged Navier-Stokes (RANS) equations is a common practice. The standard k-ε and RNG k-ε turbulence models showed good performance in predicting the flow fields [7, 8, 21], though the baseline k-ω turbulence models [6] and large-eddy simulation (LES) are also adopted in some studies [19, 20]. It should be noted that numerical simulation needs to be verified against experimental data.

Street canyon is the basic unit of urban building arrangement. Numerous studies of flow and

pollutant distribution in canyons have been carried out extensively and thoroughly. These studies include but are not limited to the impacts of canyon's aspect ratio of leeward building height and the street width (AR) [22], roof shape [23], computational settings [24], source positions [25], building wall heating [26] and various treatment of turbulent flow [27]. AR plays a significant role in determining the canyon's flow pattern. Three distinct flow regimes exist in canyons namely isolated roughness flow regime (AR<0.3), wake interference flow regime (0.3<AR<0.7) and skimming flow regime (AR>0.7) [28]. However the above conclusion is valid for flat roof buildings.

When roof shape changes to triangle, arch, trapezoid or others [23, 29, 30], the flow becomes quite complex. Unlike the discussion of AR impact, it seems difficult to summarize flow pattern influenced by roof shape. For canyons with the same roof shape on both sides, the single vortex appears in the canyon with downward wedged roofs, while upward wedged roofs lead to double vortices [30]. When the roof is slanted, the roof slope of 18° is found to be the switching point between a one- and a two-vortex regime in the canyon under the certain settings [23]. However for canyons with different roof shapes on two sides, these conclusions are not valid. Roof shape indeed alters the canyon's flow dramatically, and systematic and thorough research is few so far.

Currently there are rare reports on the coupling of air flow in and out of the roadside buildings of street canyon [7, 8]. The influence of the window-opening-percentage (1%, 3%, 5%, 10%) and building arrangement (regular and staggered) was evaluated for the canyons with flat roofs [7, 8]. The impact of roof shape on flow structures is already complex for canyons composed of solid buildings. Then its effects on the coupling flows in and out of buildings should be more difficult and have not been considered up to now.

As mentioned above, roof shape influences the number and distribution of vortices within street canyons. This should be attributed to the air pressure change caused by roof shape. It is then possible that the ventilation through windows on building walls could also be influenced. Additionally, opening windows makes the building no longer a solid structure, thus the flow patterns in the canyon are possible to be affected by the airflow through windows. For better indoor air quality, it is worth investigating whether the roof shape can be used to control the window ventilation. Therefore, the paper aims to study the impact of roof shape on flow structures and pollutant diffusion in and around buildings within street canyons using CFD technique.

Materials and methods

Building geometries and settings

Referring to the wind tunnel experiment of street canyon [31], the modified 5-storey building model with indoor partitions is showed in Fig.1. The geometric model scale is 1:83, as the model building height H=180 mm corresponds to a typical 5-storey building height H_n=15 m in urban areas. Considering the subsequent numerical model validation is conducted on the basis of the wind tunnel experiment, scaled model instead of full-scale buildings is chosen to ensure more credibility of simulation.

There are a total of 8 elongated building models with the same size 180 mm (H) ×180 mm (W) ×2250 mm (L). The target canyon is formed by B1, B2 and the street between them. To realize the fully developed turbulence effect, 5 buildings are arranged upstream, named U1 to U5 respectively, building is set downstream.

Due to the limitation of computation resources, only the central parts of B1 and B2 are replaced with ventilated buildings (the light gray part

in Fig.1. The ventilated parts are arranged in a mirrored manner along the symmetry plane (x=0.9m) of the canyon. On each floor of B1 and B2, there are five units. They are all divided into three connected rooms by Wall-B and Wall-C (see Fig. 2). All walls have a thickness of 4 mm. In the paper, unit ventilation is realized by the circular windows (d=15 mm) on walls. To investigate the effects of different ventilation resistance, five types of window arrangements are considered in the study, namely type-I, type-C, type-P, type-SS, and type-LS (see Fig. 2). Obviously type-I provides the minimum flow resistance while type-LS the maximum.

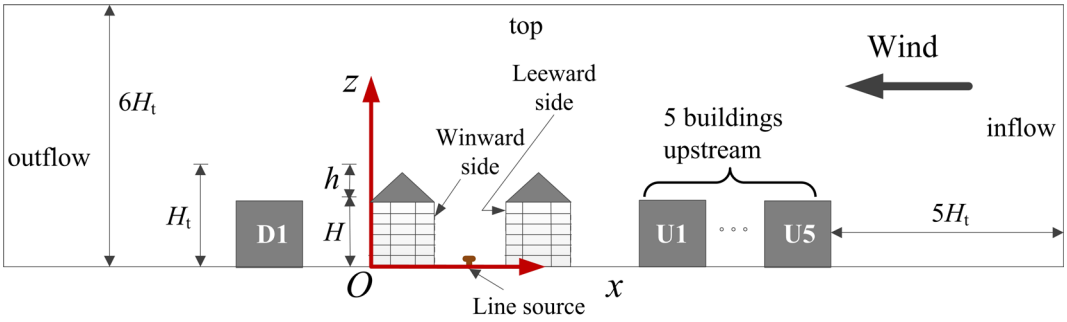

(a) Side-view of computational domain

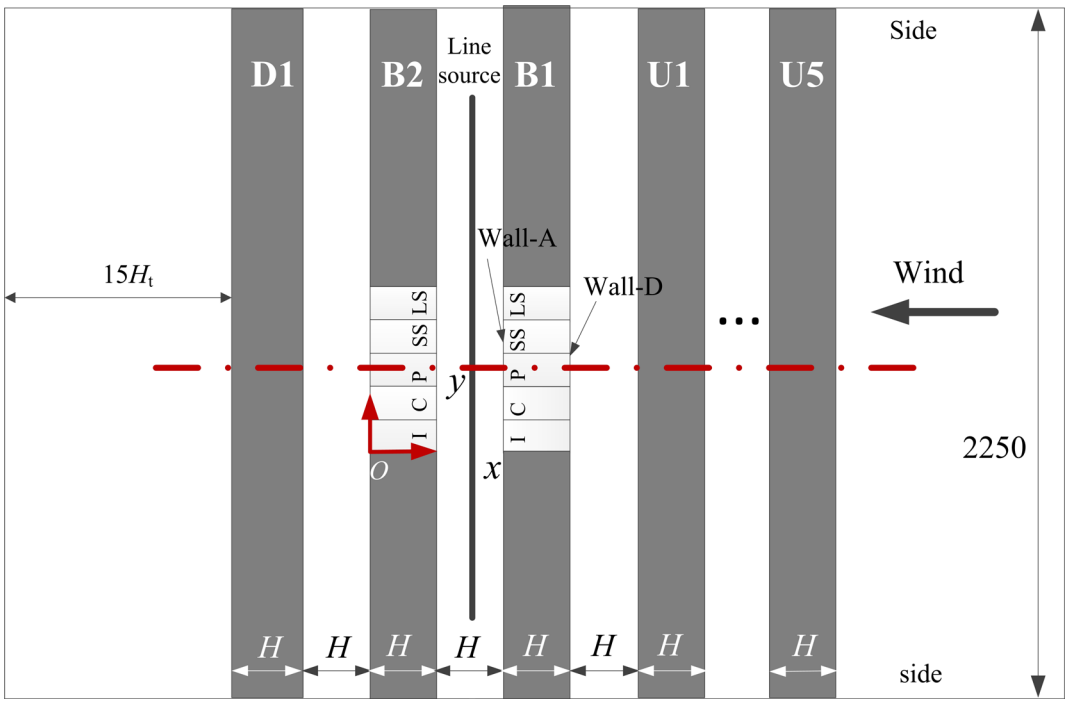

(b) top-view of computational domain

Fig. 1. Settings of computational domain

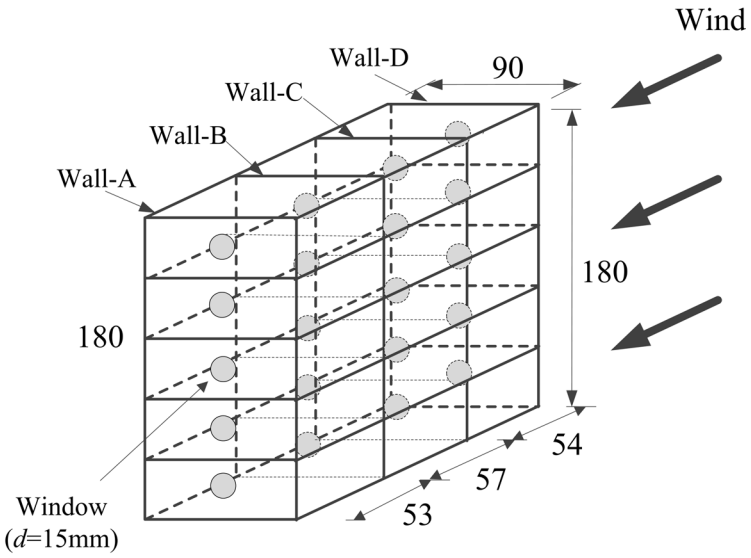

(a) Building model with type-I ventilation of B1

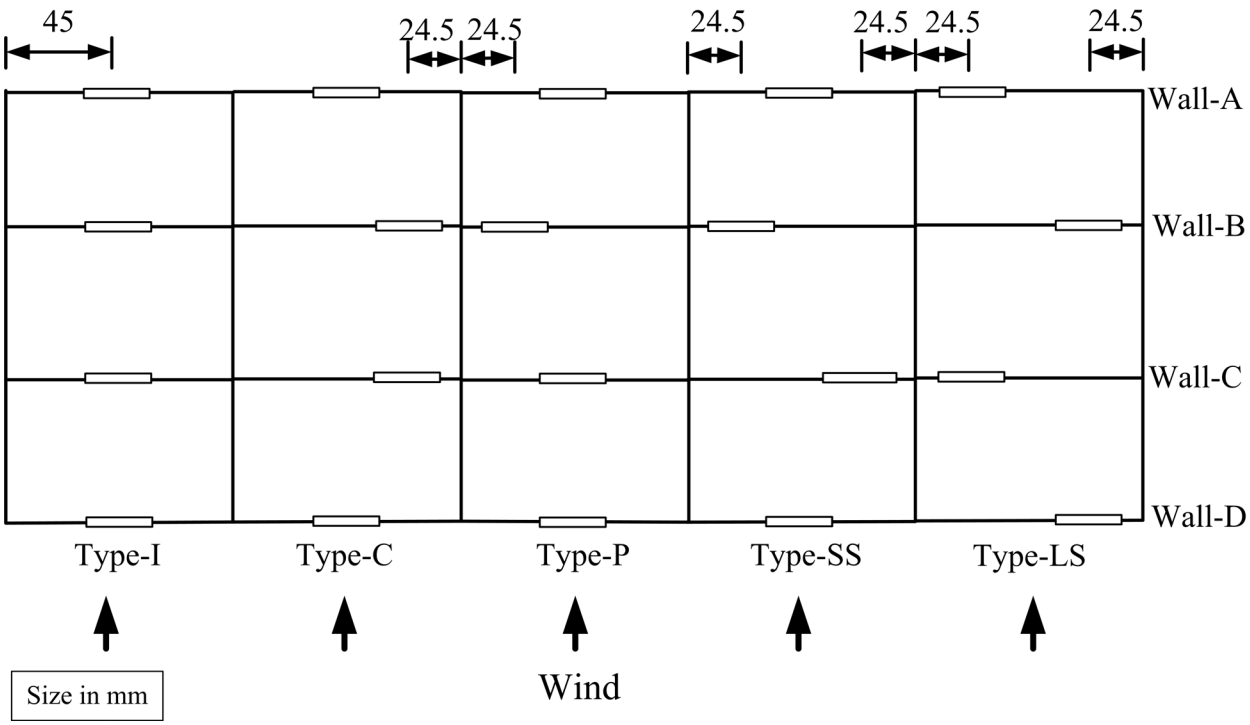

(b) Top view of each floor in the central part of B1

Fig. 2. Settings of the cross-ventilated building model

Table 1. Case Naming and description

No.	Name	Triangle roof height (mm)
1	FF	0
2	TT-30	30
3	TT-45	45
4	TT-60	60
5	TT-75	75
6	TT-90	90

Besides the flat roof, the isosceles triangular roofs with various height of h (30 mm, 45 mm, 60 mm, 75 mm and 90 mm) are considered in simulation. Triangular roof is common for many multi-story buildings in cities. Compared with the flat roof, the triangular roof can provide better insulation and avoid rainwater leakage for the top floor. Hence the paper chooses this roof shape to study its impact on the canyon's flow.

Table 1 is the summary of the cases in the paper. The line source is located in the middle of the street (see Fig. 1). The source strength and geometry size is set according to the wind tunnel experiment [31].

Numerical model

For simulation of airflow coupling indoors and outdoors, the RANS-based modeling approach is more suitable than the large eddy simulation model, which requires more computational power and resources. The transport of averaged flow quantities are governed by the RANS equations, and turbulence effects produced by certain scale range of eddies are determined by selecting appropriate turbulence model. In the paper, RNG k-ε turbulence model is employed. The model is built with the additional term in ε equation and inclusion low-Reynolds number and swirl effects. These improvements make the RNG k-ε model perform better than the standard k-ε model in simulating of rapid strain, swirling and other flows. In the previous studies, RNG k-ε model has also been proved to have good predictive ability in flows around buildings [21, 24, 32]. The region near wall is treated by the standard wall function. This can obviate the need to resolve the viscosity-affected region. Hence the grid near wall is allowed to be relatively coarse. Due to gas pollutant is treated as passive scalar, its transmission and distribution is solved by species transport equation. Additionally, the airflow is incompressible for the influence of sunshine on air temperature is not considered.

The settings of computational domain (see Fig.1) conform to the CFD guidelines [33]. In domain discretization, three types of meshes, namely the coarse, medium and fine meshes, are chosen to obtain the grid-independent solution by using ANSYS ICEM. The size of the first layer near

the wall is taken as about 8 mm, 6 mm and 5 mm indoors while 12 mm, 10 mm, 8 mm outdoors respectively. In the zone of windows, the grid size is refined to about 3 mm, 2 mm and 1.5 mm respectively. Grid sensitivity analysis is conducted for case FF with these three types of mesh. To compare the simulation difference, the dimensionless ventilation rate, Q^0, is used. The detailed definition of Q^0 is given in the following section of Results and Discussion. Fig.3 depicts a comparison of Q^0 for type-I and type-LS windows. There are no observable differences between the simulation results among the three grids. The difference in quantity is approximately within 5%. Therefore the resolution of the medium mesh is considered sufficient and the following results are all given based this type of mesh, whose total number is about 1×10^7~1.5×10^7 for all cases.

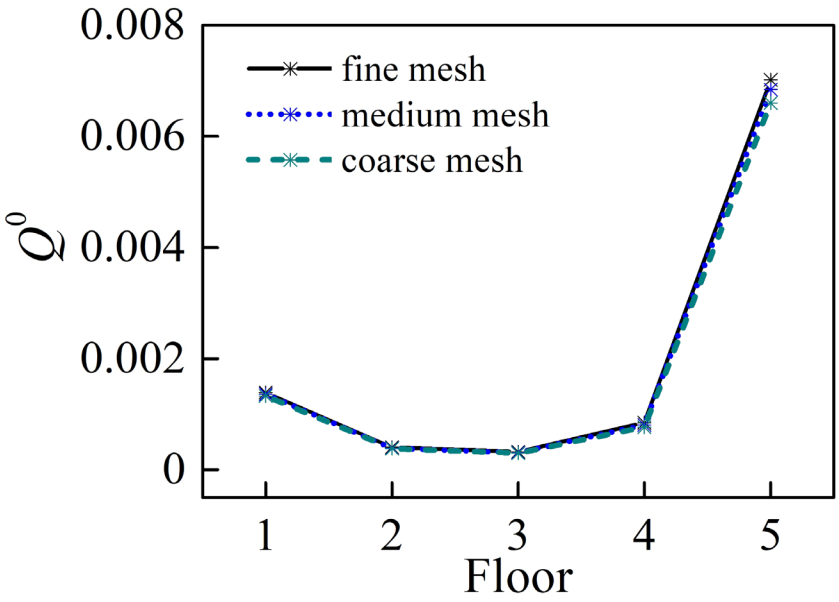

(a) Q^0 of type-I windows on wall-A in B1

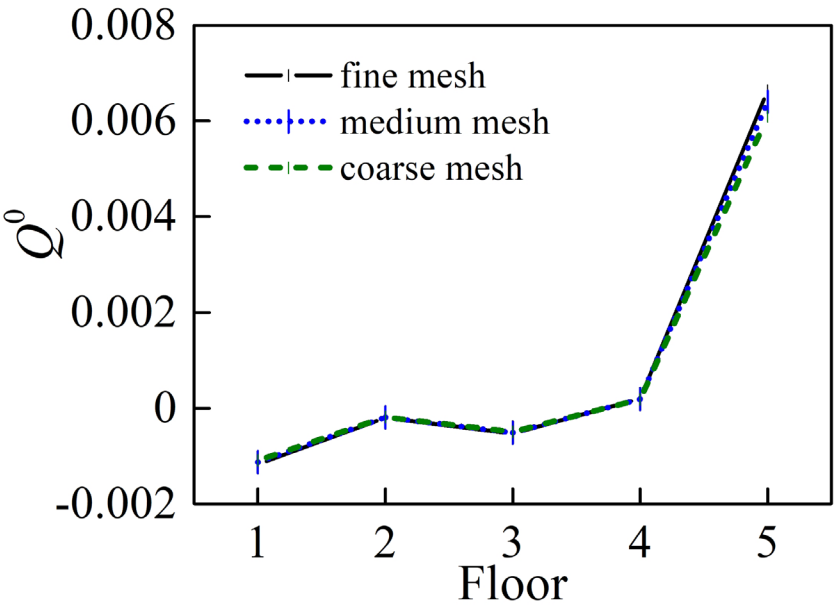

(b) Q^0 of type-LS windows on wall-A in B2

Fig. 3. Q^0 of windows under three types of mesh in FF

The boundary conditions are set as follows. On building walls and floors, no-slip conditions are used. As the study is carried out based on the wind tunnel experiment [31], the lateral sides of the computational domain are also set as walls. The top is specified as symmetric condition as normal gradients of all variables are assumed zero. At the inflow, a power law velocity profile is employed with the formula as $u=U_r\times(z/H)^{0.25}$, where U_r=3.5m/s. The turbulence intensity is set as 2.5%. The inflow conditions are given according to the velocity profile of the wind tunnel of the University of Shanghai for Sci. &Tech, and the present simulations are expected to be verified in the tunnel. Moreover, the Reynolds number (UrH/v) exceeds the value of 3400, which ensures the flow patterns in the canyons are independent of the viscous effects [34]. For the outlet of the computational domain, the outflow condition is applied.

In solving the governing equations with ANSYS Fluent (version 13.0), the SIMPLE algorithm is selected. Convection terms are discretized using the second-order upwind scheme to avoid false diffusion caused by low order formats. Generally the requirement of scaled residuals is less than 10^{-3}. To ensure the convergence, the criterion in the present study is set as being less than 10^{-5}. At the same time, the monitored representative flow and pollutant variables should remain unchanged when the iteration continues.

Numerical model validation

To ensure the reliability of CFD results, the numerical model needs to be validated by measurements. Simulating building ventilation requires consideration of three-dimensional flow. Therefore, the pollutant concentration measurement of 3D isolated street canyon performed in the wind tunnel of University of Karlsruhe [31] is adopted to verify the numerical model in the paper. In the experiment, the canyon of $H_0\times W_0\times L_0$ (W_0: street width; H_0: building height; L_0: building length) 120 mm×120 mm×600 mm was constructed by the two same rectangular buildings BI and BII with the spacing of 120 mm (see Fig. 4). Thus the aspect ratio of the canyon equals one. On the windward and leeward of the canyon, the measuring points are distributed on 6 vertical line segments, which are evenly arranged with the distance of $1.25H_0$. In Fig. 4, the three canyon sections of $y=1.25H_0$, $y=2.5H_0$, and $y=3.75H_0$ are named as S1, S2, and S3 respectively. Hence the positions of the line segments can be named as S1-lee, S1-win and so on. The incoming flow direction was perpendicular to the axis of the canyon.

The computational domain is set according to the wind tunnel dimensions (see Fig. 5). The top of the domain is $6H_0$ above the ground. At the inflow, the velocity profile is $u=U_{ref}\times(z_{ref}/H_0)^{0.23}$, where U_{ref}=7.7m/s, z_{ef}=0.667m [31]. The other boundary conditions are the same as the settings in the section of numerical model.

As for the ground traffic line source, it is fixed close to the leeward of the street canyon (see Fig. 5). A mixture of SF_6 and air is used to simulate gaseous vehicle pollutants. In this paper, the volume fraction of SF_6 named as c is dimensionless treated according to $K_{SF6}=c\times U_{ref}\times H_0\times L_s/Q_s$, where L_s is the length of the line source (m) and Q_s is the source rate (m^3/s). The specific settings of the source can be referred to the wind tunnel experiment [31].

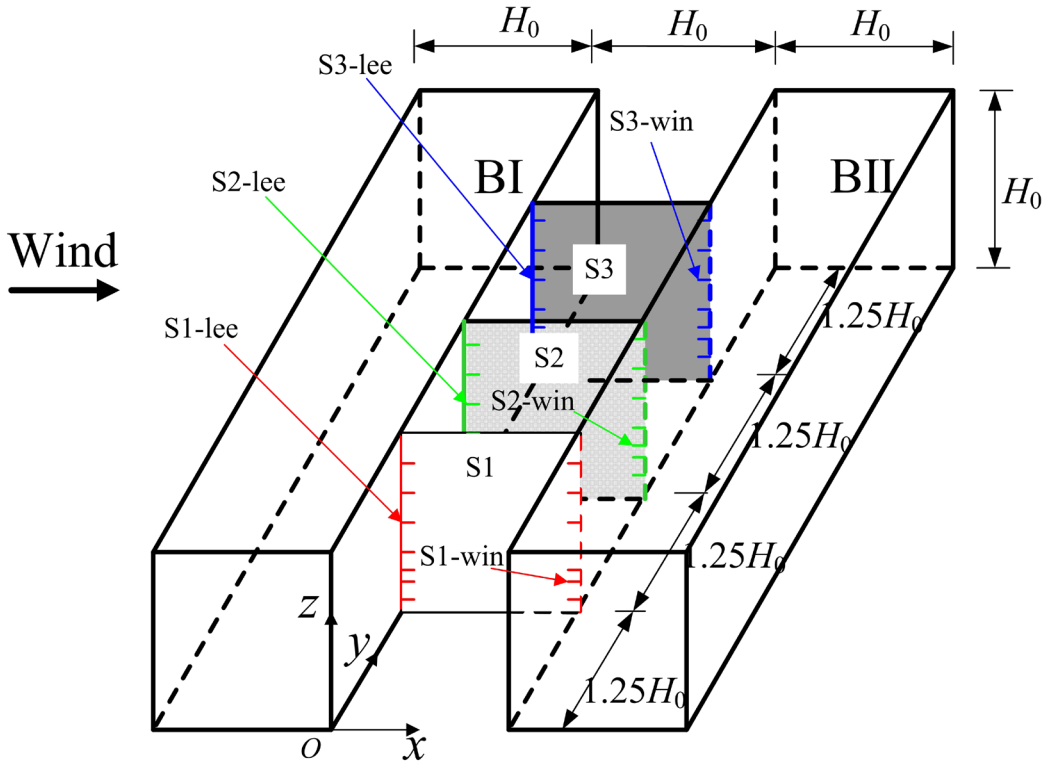

Fig. 4. Distribution of measuring points in the validation case

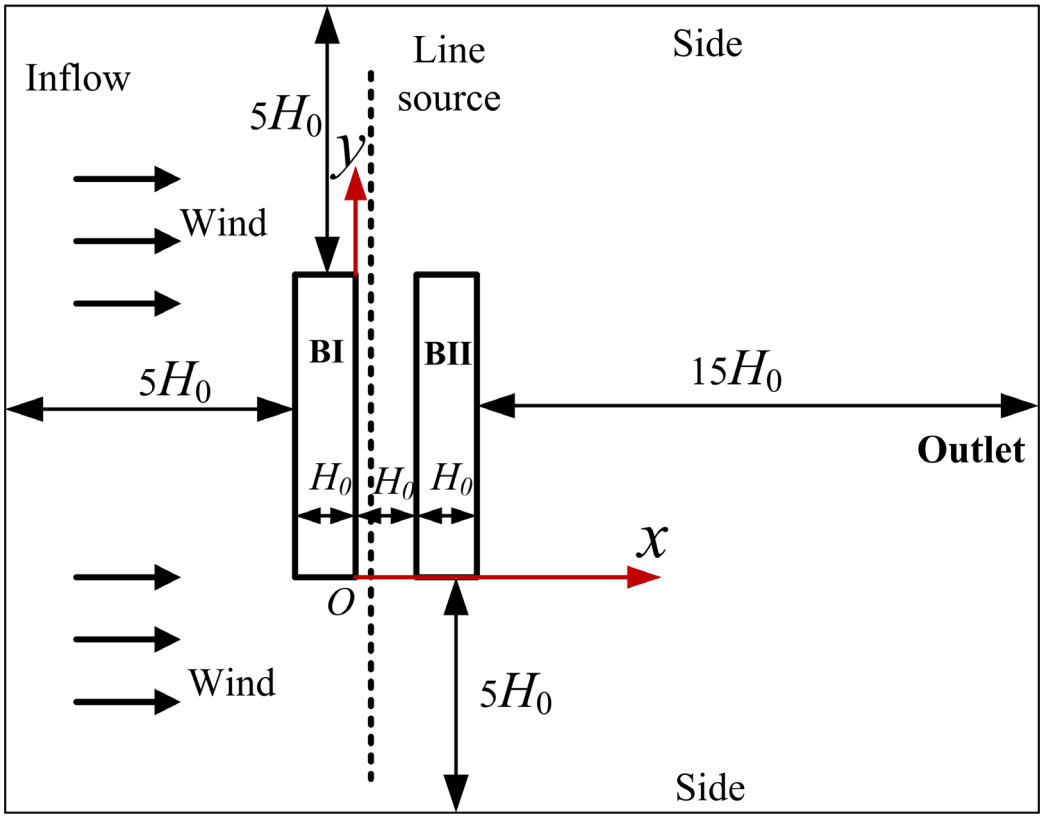

Fig. 5. Computational domain for the validation case

Fig. 6 shows K_{SF6} comparison between the simulated and the wind tunnel measurement on leeward and windward walls. It can be seen that the simulated K_{SF6} is fairly matches with the measured ones. For the street canyon with AR equaling one, a great number of reports have demonstrated that the main vortex transports the ground traffic pollutants, causing the higher level near the leeward than that near the windward [8, 9, 23, 24, 27, 31]. The simulated and test results both agree with the conclusion. Additionally the pollutant concentration difference between S1 and S3 is negligible. Fig. 6 also shows that K_{SF6} on the midstream surface S2 is slightly larger than that on S1 and S3 at the same height, which indicates that when L equals 5H, the concentration distribution has shown the characteristics of 2D flows. The concentration on the cross section of street canyon basically does not change with the street length.

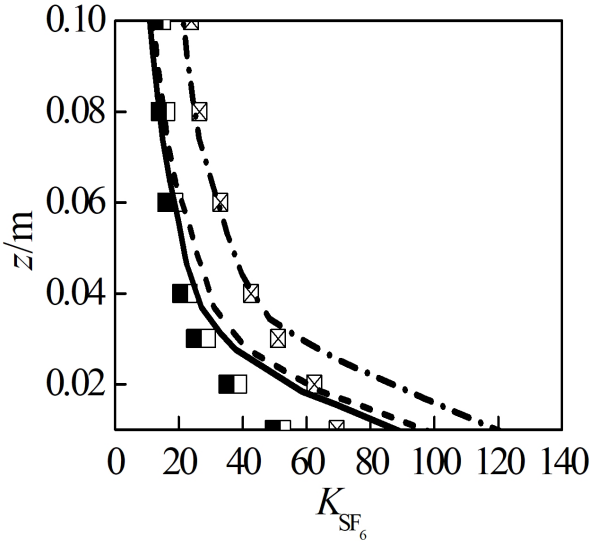

(a) Leeward

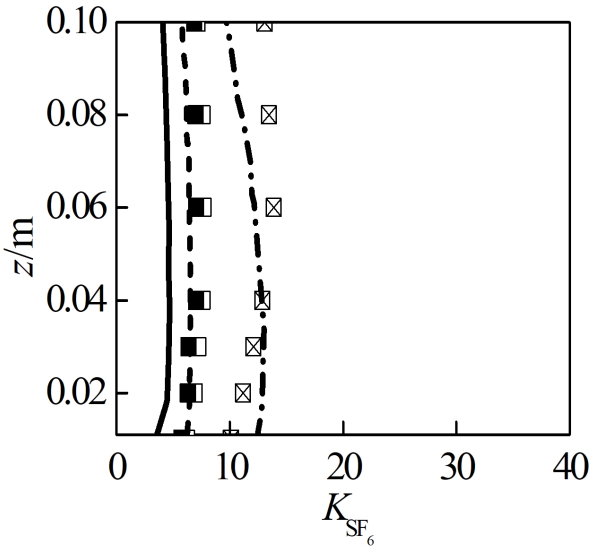

(b) Windward

□ Measured K_{SF6} on S1[31] □,× Measured K_{SF6} on S2[31] ■ Measured K_{SF6} on S3[31]
⋯⋯ Simulated K_{SF6} on S1 —·— Simulated K_{SF6} on S2 —— Simulated K_{SF6} on S3

Fig. 6. K_{SF6} distribution on building walls in street canyon

As shown in Fig. 6, K_{SF6} on the leeward decreases with height, and the maximum occurs near the ground. When z>0.03 m, the simulated are basically the same as the measured, but near the ground the simulated K_{SF6} are higher than the experimental data. On the windward side, K_{SF6} are relatively small and remain basically unchanged with height. The K_{SF6} discrepancy on the leeward near the ground could be attributed to two reasons. One is experimental errors. The sampling devices near the ground inevitably interfere with the flow and pollutant diffusion around. However, the device effect is not considered in numerical simulation. The other reason is computational errors caused by the discretization scheme and the turbulence model.

A comprehensive validation should cover both flow and concentration fields, thus ensuring the model's reliability and accuracy as much as possible. Due to the lack of experimental flow data, the present study could not directly evaluate the accuracy of the simulated mean velocity and fluctuations. Considering the gas pollutant is treated as passive scalar, the good K_{SF6} agreement indicates that the flow prediction is basically correct.

The above analysis proves that the simulation method adopted in the paper is fairly good in predicting flow and pollutant distribution in 3D street canyon.

Results and discussion

Considering the focus of the paper is not on the detailed indoor flow but the impact of roof shape on indoor air quality, the wind and concentration fields are given only for type-I and type- LS (Fig. 7 to Fig. 12). The two types are chosen for they represent the minimum and maximum flow resistance respectively. For type-I, the displayed is the symmetrical plane (y=0.045 m, see Fig. 1 and Fig. 2) of the room, while for type-LS the plane is taken through the middle position of the windows on Wall-A and Wall-C (y=0.3845m, see Fig. 1 and Fig. 2). In all cases, the dimensionless ventilation rate Q^0 ($Q/(u_H \times 0.5H \times 0.2H)$ are presented, that is, the reference area is computed by the windward area of the unit. When the airflow through the window is consistent with the incoming wind direction, the Q^0 is plus, otherwise it is negative.

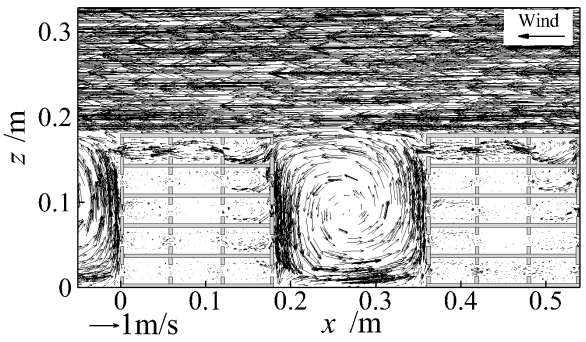

Flow field of type-I at y=0.045m

(a)

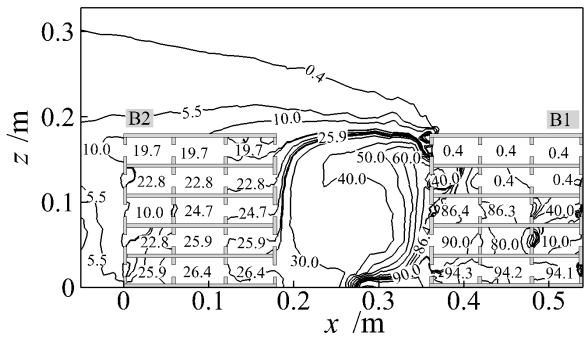

K_{SF6} contour of type-I at y=0.045m

(b)

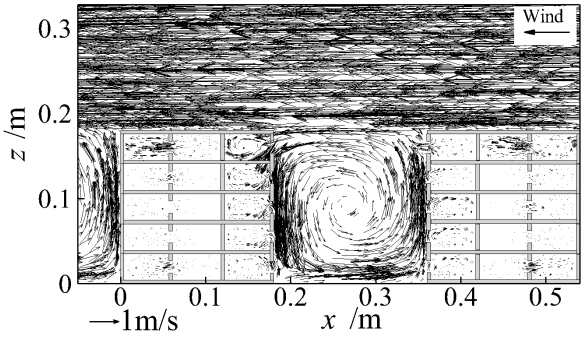

Flow field of type-LS at y=0.3845m

(c)

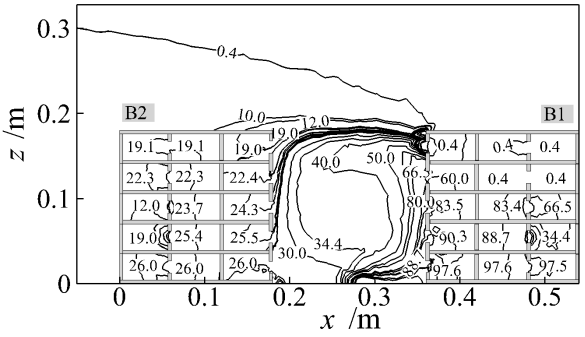

K_{SF6} contour of type-LS at y=0.3845m

(d)

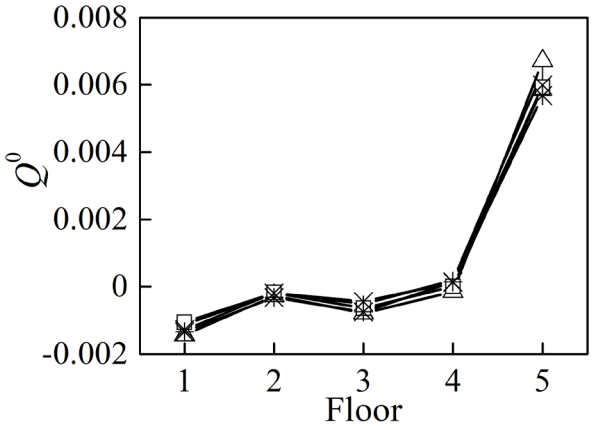

Q^0 of windows on wall-A in B1

(e)

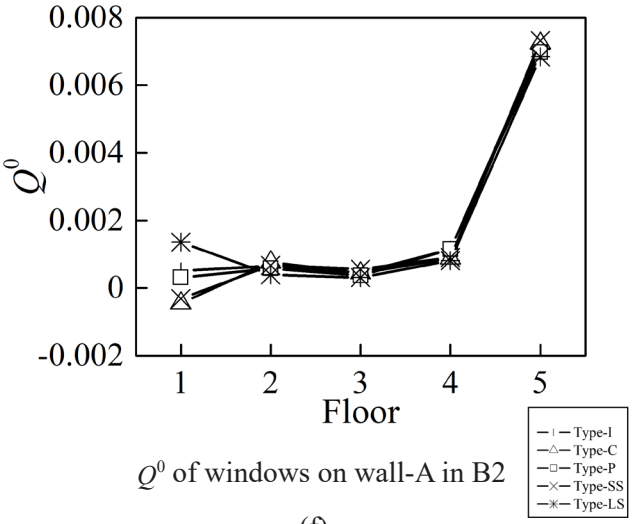

Q^0 of windows on wall-A in B2

(f)

Fig. 7. Results of FF

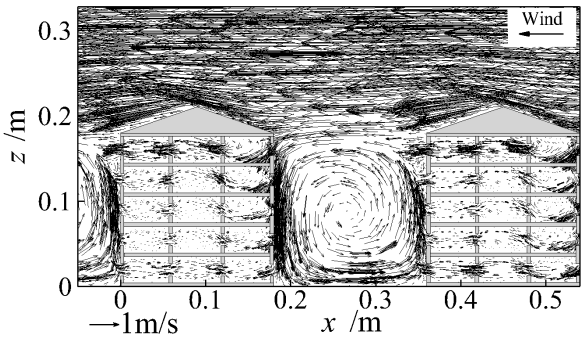

Flow field of type-I at y=0.045m

(a)

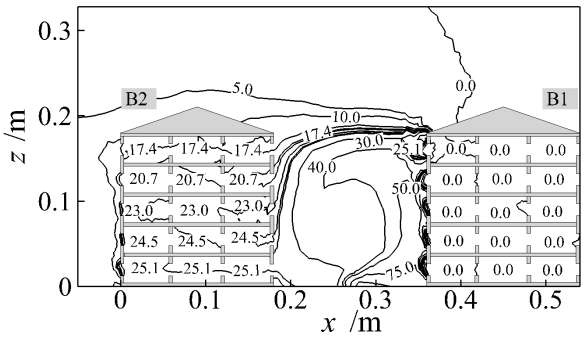

K_{SF6} contour of type-I at y=0.045m

(b)

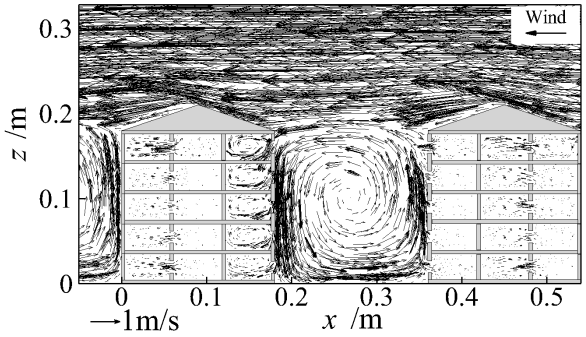

Flow field of type-LS at y=0.3845m

(c)

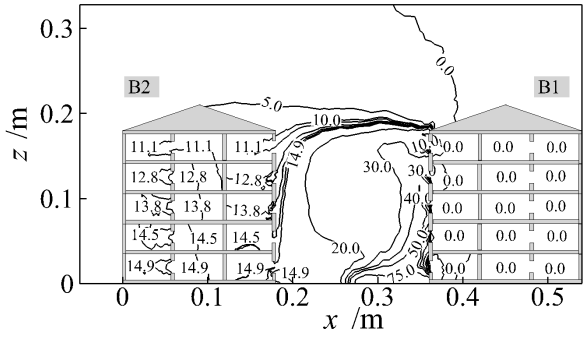

K_{SF6} contour of type-LS at y=0.3845m

(d)

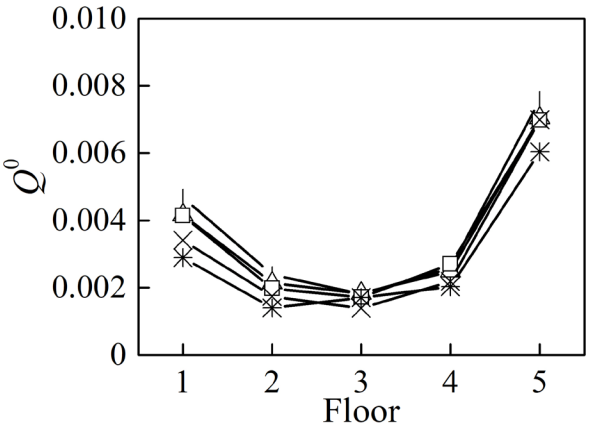

Q^0 of windows on wall-A in B1

(e)

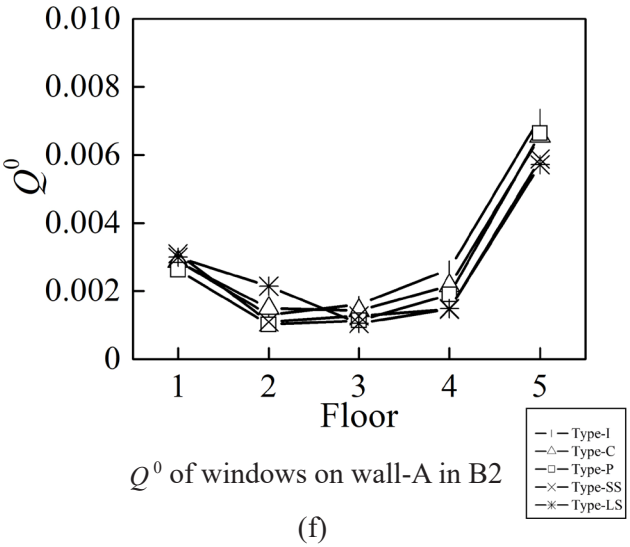

Q^0 of windows on wall-A in B2

(f)

Fig. 8. Results of TT30

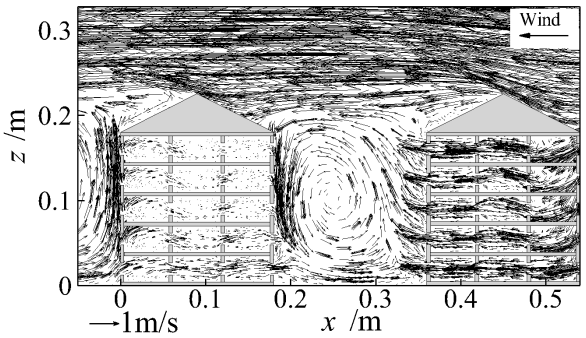

Flow field of type-I at y=0.045m

(a)

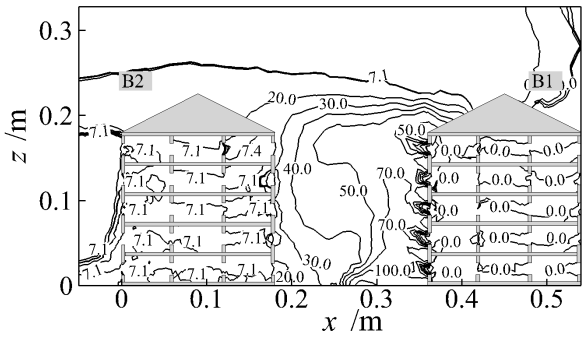

K_{SF6} contour of type-I at y=0.045m

(b)

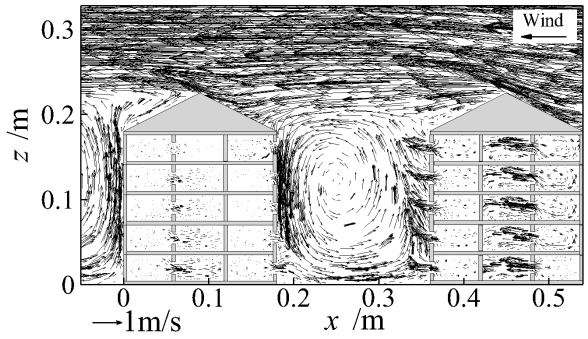

Flow field of type-LS at y=0.3845m

(c)

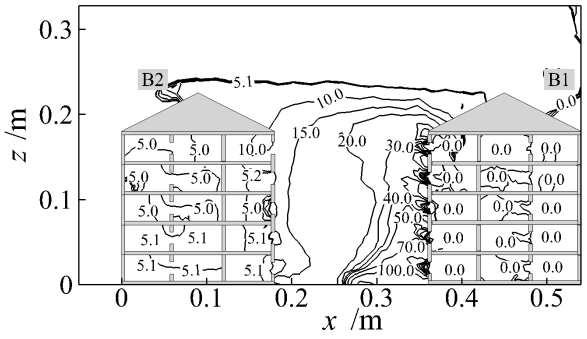

K_{SF6} contour of type-LS at y=0.3845m

(d)

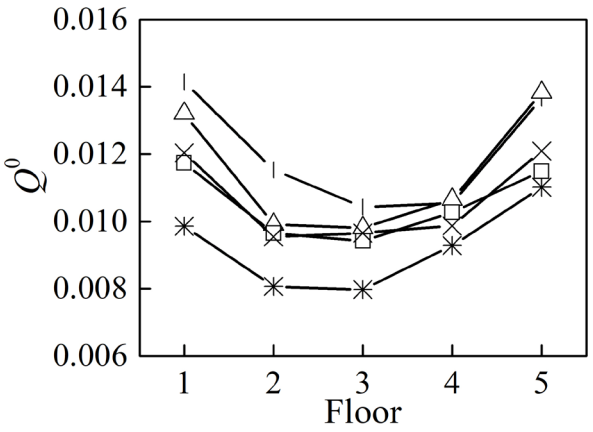

Q^0 of windows on wall-A in B1

(e)

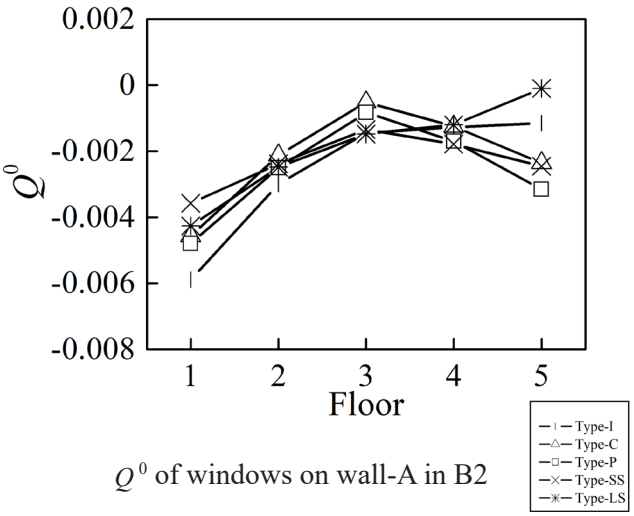

Q^0 of windows on wall-A in B2

(f)

Fig. 9. Results of TT45

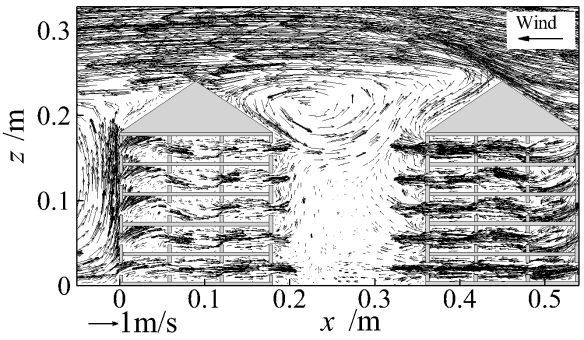

Flow field of type-I at y=0.045 m

(a)

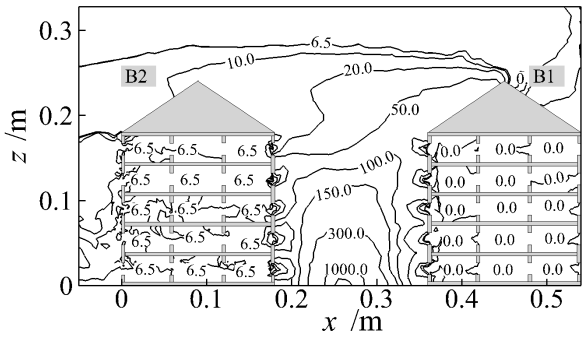

K_{SF6} contour of type-I at y=0.045 m

(b)

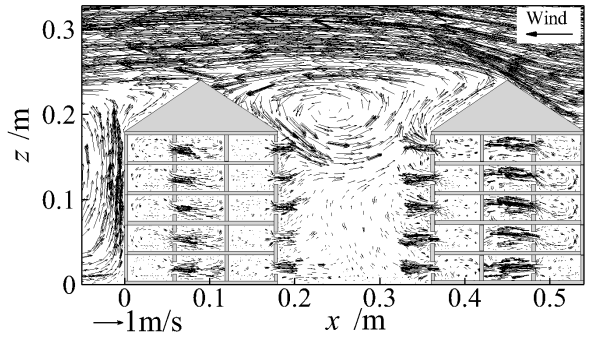

Flow field of type-LS at y=0.3845 m

(c)

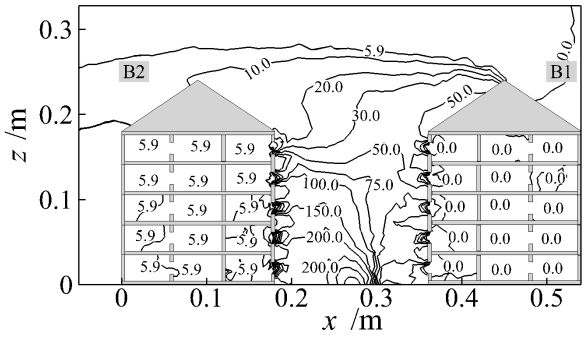

K_{SF6} contour of type-LS at y=0.3845 m

(d)

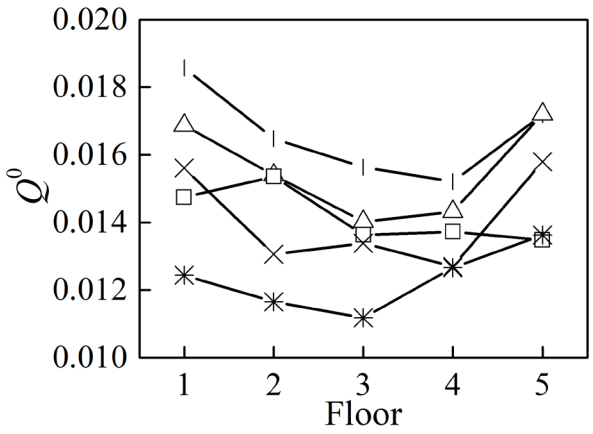

Q^0 of windows on wall-A in B1

(e)

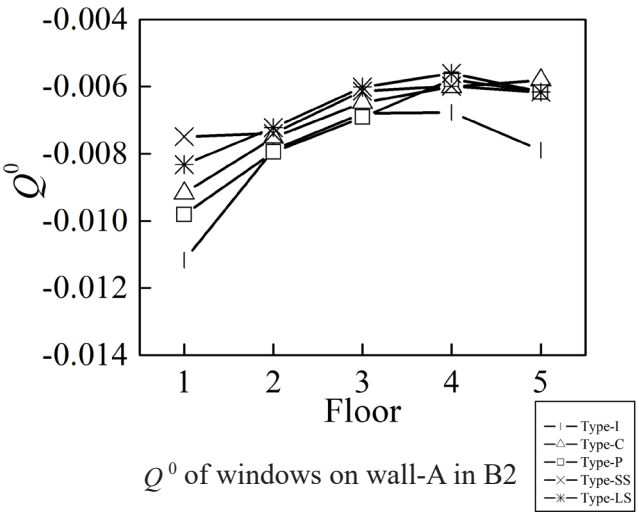

Q^0 of windows on wall-A in B2

(f)

Fig. 10. Results of TT60

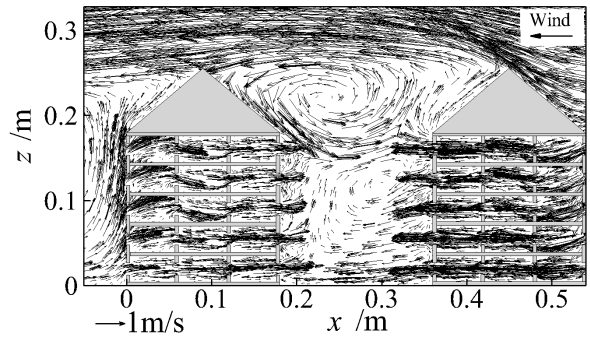

Flow field of type-I at y=0.045 m

(a)

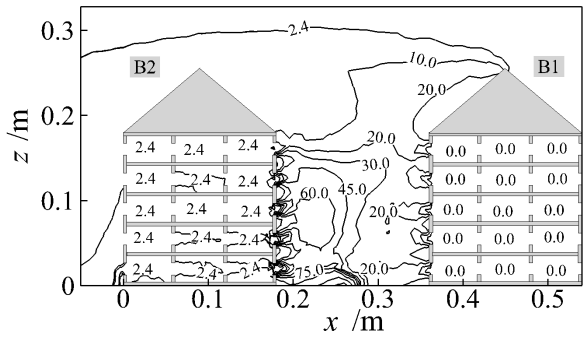

K_{SF6} contour of type-I at y=0.045 m

(b)

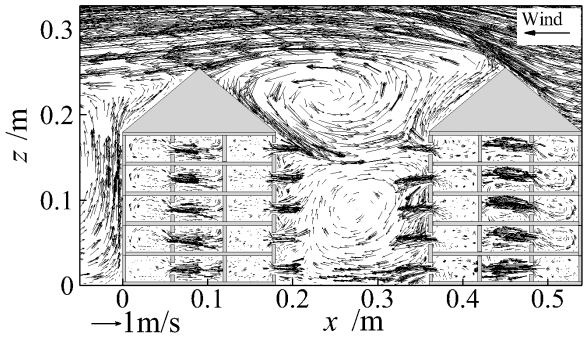

Flow field of type-LS at y=0.3845 m

(c)

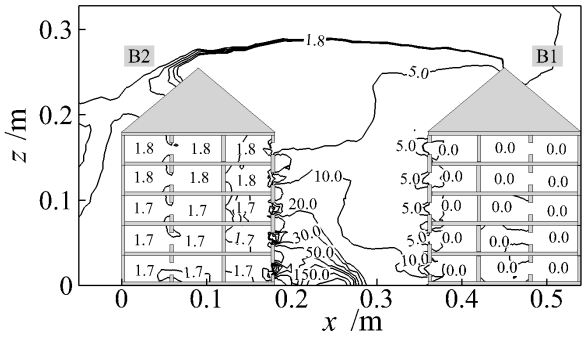

K_{SF6} contour of type-LS at y=0.3845 m

(d)

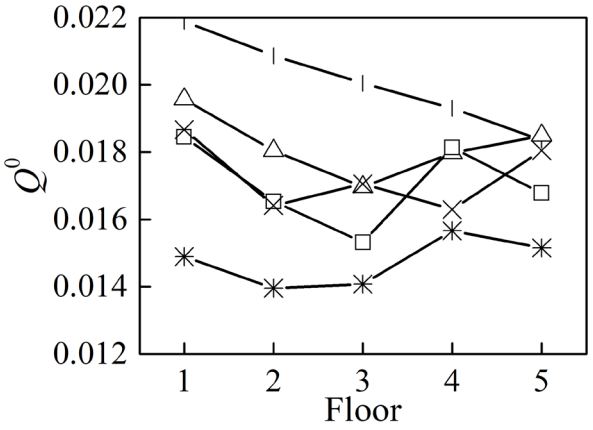

Q^0 of windows on wall-A in B1

(e)

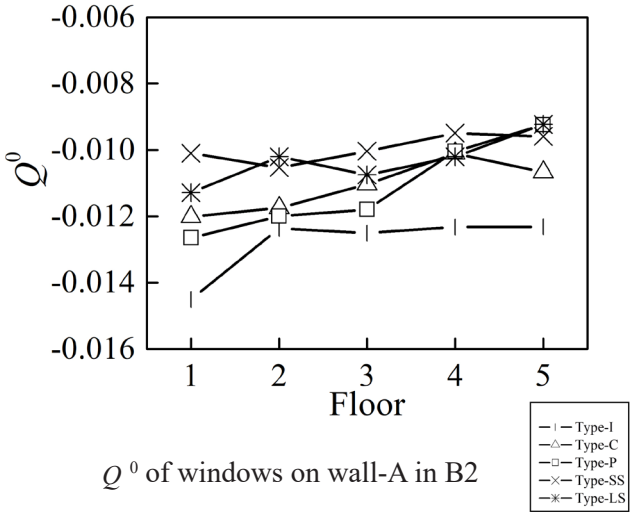

Q^0 of windows on wall-A in B2

(f)

Fig. 11. Results of TT75

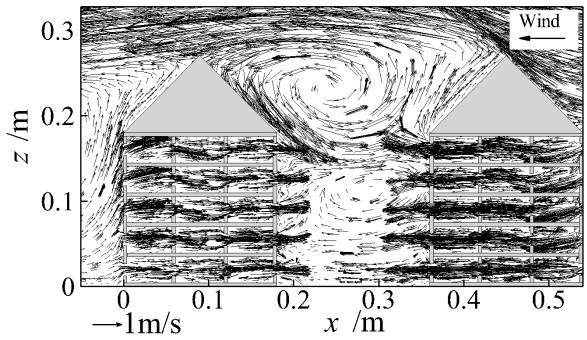

Flow field of type-I at y=0.045 m

(a)

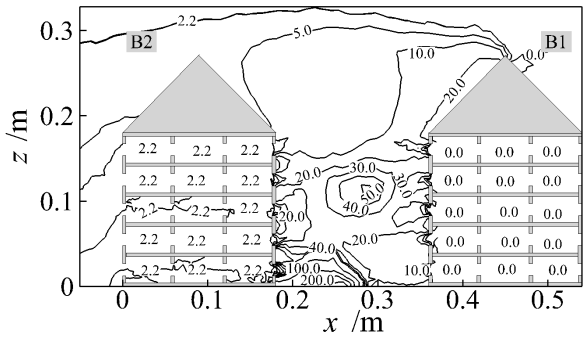

K_{SF6} contour of type-I at y=0.045 m

(b)

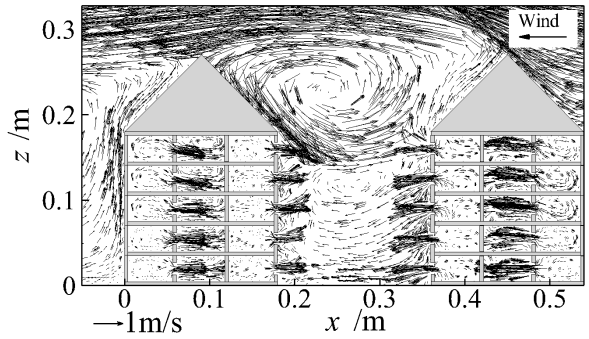

Flow field of type-LS at y=0.3845 m

(c)

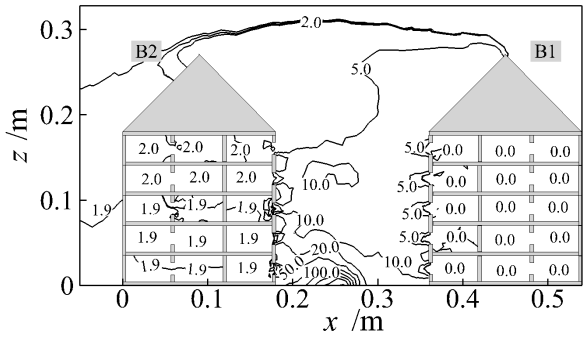

K_{SF6} contour of type-LS at y=0.3845 m

(d)

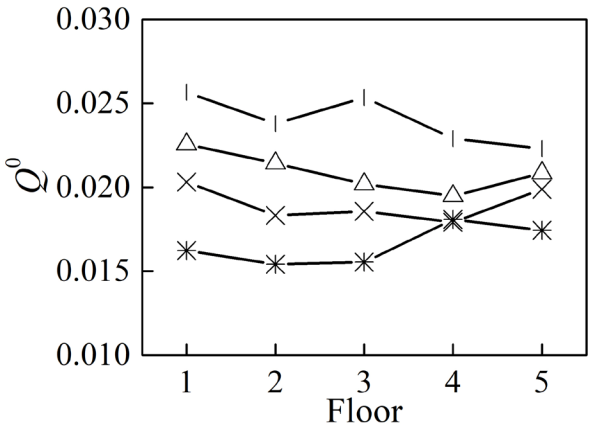

Q^0 of windows on wall-A in B1

(e)

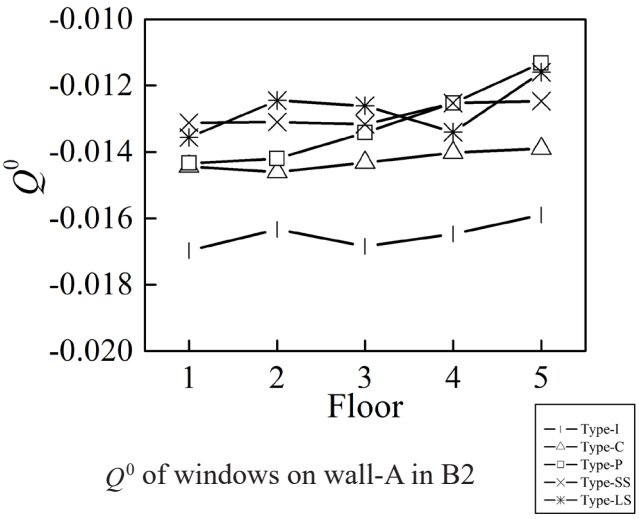

Q^0 of windows on wall-A in B2

(f)

Fig. 12. Results of TT90

General characteristics of flow and pollutant distribution outdoors

According to the vortex characteristics, the canyons' skimming flows simulated in the paper can be classified into two types. One type is that there is one main vortex, such as the flows in the canyons of FF, TT30 and TT45 (Fig.7-Fig. 9). The other type is that two adjacent contra-rotating vortices exist in the upper and lower parts of the canyon, such as the flows in TT75 and TT90 (Fig. 11-Fig. 12). The upper and larger vortex is located between two triangular roofs, while the lower and smaller one lies in the canyon within the height between the 2nd and 5th floor. As for TT60, it seems that the lower vortex does not exist (Fig. 10). However it also belongs to the second type. The reason will be given in the following text.

In previous studies for canyon of solid buildings, AR is proved to be the critical factor in determining the vortex characteristics for the flat-roofed street canyon with symmetry structure [35, 36]. The threshold value of AR is about 1.538-1.667 when flow changes from one to two vortex regimes [35-37]. There seems to be no reported study on this

critical value for canyons with triangular roofs. In the present study, TT60 is the switching case. If the total building height (=240mm) is used to calculate AR, the threshold value is about 1.333. For the isolated street canyon with the same roof shape and AR□the two vortex regimes is also found in the wind tunnel experiment [31]. It can to some extent prove that the critical value of the present study is basically reliable. The decrease of the threshold value should be attributed to the slopes of triangular roofs. These slopes make the upper vortex develop more easily and also keep the position of the vortex unchanged (Fig. 10-Fig. 12). On the contrary, the lower vortex is unstable. Its shape and position change with the roof height. However the lower vortex is also influenced by the air flows through the windows adjacent to the canyons.

The gaseous pollutant distribution is strongly dependent on the type of flow regime inside the canyon. In the cases of FF, TT30 and TT45 (see Fig. 7-Fig. 9), the pollutant is transported by the main vortex, resulting in K_{SF6} near the leeward of B1 is much larger than that near windward of B2. The distribution is similar to that of the validation case. As two vortices occur in the cases of TT75 and TT90, K_{SF6} near the windward is much larger than that near leeward. It agrees with the characteristics of pollutant distribution in the studies of deep flat-roofed street canyons [22, 25]. Fig. 11 and Fig. 12 show that it is the lower vortex that carries pollutant to the windward side. For TT60, the flow in the lower part is weak. The K_{SF6} level near the windward side is also higher, especially for the situation of type-I (see Fig. 10).

Pollutant level and ventilation indoors under one-vortex flow regime

For case FF, K_{SF6} decreases with the building height in B1. The maximum K_{SF6} on each floor always takes place in rooms close to the wall-A. On the fifth floor, K_{SF6} suddenly changes to nearly zero. In B2, the K_{SF6} varies slightly with the height, which is the same as the K_{SF6} distribution near the windward of the canyon. Obviously the indoor distribution of K_{SF6} is not only determined by the polluted air outdoors but also by the wind direction through windows. According to Bernoulli equation for gas flow, the pressure difference between wall-A and wall-D determines the ventilation direction in each building units. The magnitude of Q^0 depends on the indoor ventilation resistance. Fig. 7 shows that Q^0 of the rooms in B1 from the first to fourth floor is small and negative. This means the polluted air near the leeward enters these rooms. However Q^0 of the fifth floor shifts to plus and the value becomes large, thus the flow there prevents the pollutant outside from entering the rooms. K_{SF6} of the fifth floor keeps at very low level. The indoor level of K_{SF6} in B2 can be explained in the same way.

Fig. 7 also shows that the difference of K_{SF6} in rooms of each floor is associated with the magnitude of Q^0. When Q^0 is close to zero, the K_{SF6} difference shows larger, such as in the rooms of the 2nd and 3rd floor (Figs. 7b and d). The closer the room is to the street canyon, the higher the concentration of the room. Whereas, when the magnitude of Q^0 is a little greater than zero, whether positive or negative, it seems no K_{SF6} difference among the three connected rooms. Hence the internal building walls could block pollutant from diffusion to some extent when there is no air convection in units. However the blocking effect disappears even in weak convective conditions, which is particularly obvious in the rooms of the first floor. Figs. 7e and f show that floor location is the main factor in determining the ventilation magnitude for FF.
In TT-30, Q^0 of all rooms turns positive due to the change of roof shape. All rooms of B1 are not contaminated. In rooms of B2, K_{SF6} decreases slightly with the height. It should be noted that K_{SF6} of B2 in TT-30 is generally lower than that in FF. Apparently this is caused by the outdoor K_{SF6}

reduction near the windward walls. The triangular roofs bring about strong ventilation of the first floor in B1. It makes the high level of pollutants diluted near the ground. Then the pollutants are transported upward by the main vortex to the canyon top. In Figs. 8b and d, K_{SF6} in B2 with type-I is about 1.6 times of that with type-LS. It means the ventilation type has an impact on K_{SF6} indoors.

In TT45, the K_{SF6} in all rooms is maintained at very low level. The type-I ventilation near the windows of B1 is so strong that they push the main vortex a little far away from B1 (Fig. 9). The Q^0 difference between the two ventilation types seems more obvious. The Q^0 in B1 is nearly twice or even 10 times that of B2 for the same ventilation type and floor. It is worth mentioning that Q^0 of the first floor are the largest or the second largest in all floors for all ventilation types. This indicates that the ventilation of the ground floor is better than that of the upper floors. In TT-45, ventilation types play remarkable impact on Q^0 besides the factor of floor.

Pollutant level and ventilation indoors under two-vortex flow regime

As the roof height increases to 60 mm-90 mm (see Fig. 10-Fig. 12), the flow structure in the canyon shifted to two-vortex flow regime. In TT60, The strong airflow through the windows of B1 blows the weak vortex out of shape. Therefor the shape of the lower vortex is not clear. The phenomenon is also reported in the flat-roofed canyons [7]. In TT75 and TT90, the lower vortex is strong enough to maintain its shape. Comparing the K_{SF6} distribution of the three cases, it could be found that the ventilation types play an undeniable role in convective transport of the ground pollutants. The above analyses prove that the flow outdoors could to some extent be influenced by the flow through the openings on building walls.

The distributions of indoor K_{SF6} are nearly the same for TT60, TT75 and TT90. All rooms are almost uncontaminated. It is the result of the ventilation magnitude and directions of the windows. For the similar solid street canyon model, the pollutant level is usually higher near the ground and walls [29, 31]. Based on the conclusion, it is generally believed that indoor air would also be polluted. However, the present study shows that the window flows could effectively block the outdoor pollution.

The simulation shows that Q^0 increases with the roof height. When h is 90mm, the ventilation rate of each floor in B1 and B2 reaches its maximum in all cases. In TT90, Q^0 does not vary with the floor significantly, and ventilation type now becomes the primary factor. Overall, Q^0 in B1 is larger than that of B2. The simulation also shows Q^0 difference caused by ventilation type is more distinct in B1.

Conclusion

The paper numerically investigates the impact of roof shape on indoor air quality in a street canyon using RNG k-ε turbulence model. The conventional street canyon model is modified by replacing part of the solid building with naturally ventilated multi-story building. Based on the wind tunnel experimental data□the numerical model employed is validated. Compared with flat roofs when aspect ratio of street canyon equals one, triangular roofs would strengthen indoor ventilation as well as change the flow direction through windows. Meanwhile the strong air currents from buildings could in turn alter the fields of flow and pollutant in street canyon to some extent, thus dispersing or accumulating pollutant near the leeward or windward walls. In the paper the ventilation resistance shows undeniable impact not only on indoor ventilation rate but also on flow near the external walls. The study reinforces the importance of coupling of air flow in and out of the roadside buildings to obtain

an accurate indoor air quality.

Financial supports

This study did not receive any supporting funds from any financial resource.

Competing interests

The authors declare that there are no competing interests.

Acknowledgements

We would like to thank Prof. Baoqing Deng in Department of Environmental Science and Engineering for his insight on this project.

Ethical considerations

Ethical issues (Including plagiarism, Informed Consent, misconduct, data fabrication and/or falsification, double publication and/or submission, redundancy, etc.) have been completely observed by the authors.

References

1. Tognon G, Marigo M, De Carli M, Zarrella A. Mechanical, natural and hybrid ventilation systems in different building types: Energy and indoor air quality analysis. Journal of Building Engineering. 2023 Jun 10:107060.

2. Zhong HY, Sun Y, Shang J, Qian FP, Zhao FY, Kikumoto H, Jimenez-Bescos C, Liu X. Single-sided natural ventilation in buildings: a critical literature review. Building and Environment. 2022 Mar 15;212:108797.

3. Li H, Huang W, Qian Y, Klemeš JJ. Air pollution risk assessment related to fossil fuel-driven vehicles in megacities in China by employing the Bayesian network coupled with the Fault Tree method. Journal of Cleaner Production. 2023 Jan 10;383:135458.

4. Ai ZT, Mak CM. From street canyon microclimate to indoor environmental quality in naturally ventilated urban buildings: Issues and possibilities for improvement. Building and environment. 2015 Dec 1;94:489-503.

5. MOEEP (Ministry of Ecology and Environment Protection of China). China Vehicle Emission Control Annual Report. Beijing, China. 2014-2019. Available from: https://www.mee.gov.cn/h jzl/sthjzk/ydyhjgl/.

6. Wang J, Huo Q, Zhang T, Wang S, Battaglia F. Numerical investigation of gaseous pollutant cross-transmission for single-sided natural ventilation driven by buoyancy and wind. Building and Environment. 2020 Apr 1;172:106705.

7. Yang F, Gao Y, Zhong K, Kang Y. Impacts of cross-ventilation on the air quality in street canyons with different building arrangements. Building and Environment. 2016 Aug 1;104:1-2.

8. Yang F, Kang Y, Gao Y, Zhong K. Numerical simulations of the effect of outdoor pollutants on indoor air quality of buildings next to a street canyon. Building and Environment. 2015 May 1;87:10-22.

9. Abhijith KV, Kukadia V, Kumar P. Investigation of air pollution mitigation measures, ventilation, and indoor air quality at three schools in London. Atmospheric Environment. 2022 Nov 15;289:119303.

10. Zhou F, Niu M, Zheng Y, Sun Y, Wu Y, Zhu T, Shen F. Impact of outdoor air on indoor airborne microbiome under hazy air pollution: A case study in winter Beijing. Journal of Aerosol Science. 2021 Aug 1;156:105798.

11. Ji W, Zhao K, Zhao B. The trend of natural ventilation potential in 74 Chinese cities from 2014 to 2019: Impact of air pollution and climate change. Building and Environment. 2022 Jun 15;218:109146.

12. United Nations. World Urbanization

Prospects 2018-Highlights. Department of Economic and Social Affairs. Population Division. 2019.

13. Tominaga Y, Blocken B. Wind tunnel experiments on cross-ventilation flow of a generic building with contaminant dispersion in unsheltered and sheltered conditions. Building and Environment. 2015 Oct 1;92:452-61.

14. Golubić D, Meile W, Brenn G, Kozmar H. Wind-tunnel analysis of natural ventilation in a generic building in sheltered and unsheltered conditions: Impact of Reynolds number and wind direction. Journal of wind engineering and industrial aerodynamics. 2020 Dec 1;207:104388.

15. Ji L, Tan H, Kato S, Bu Z, Takahashi T. Wind tunnel investigation on influence of fluctuating wind direction on cross natural ventilation. Building and environment. 2011 Dec 1;46(12):2490-9.

16. Jiang Z, Kobayashi T, Yamanaka T, Sandberg M. A literature review of cross ventilation in buildings. Energy and Buildings. 2023 May 6:113143.

17. Park JS. Long-term field measurement on effects of wind speed and directional fluctuation on wind-driven cross ventilation in a mock-up building. Building and environment. 2013 Apr 1;62:1-8.

18. Gough H, Sato T, Halios C, Grimmond CS, Luo Z, Barlow JF, Robertson A, Hoxey R, Quinn A. Effects of variability of local winds on cross ventilation for a simplified building within a full-scale asymmetric array: Overview of the Silsoe field campaign. Journal of Wind Engineering and Industrial Aerodynamics. 2018 Apr 1;175:408-18.

19. Kobayashi T, Sandberg M, Fujita T, Lim E, Umemiya N. Numerical analysis of wind-induced natural ventilation for an isolated cubic room with two openings under small mean wind pressure difference. Building and Environment. 2022 Dec 1;226:109694.

20. Arinami Y, Akabayashi SI, Tominaga Y, Sakaguchi J. Performance evaluation of single-sided natural ventilation for generic building using large-eddy simulations: Effect of guide vanes and adjacent obstacles. Building and Environment. 2019 May 1;154:68-80.

21. Cui DJ, Mak CM, Kwok KC, Ai ZT. CFD simulation of the effect of an upstream building on the inter-unit dispersion in a multi-story building in two wind directions. Journal of Wind Engineering and Industrial Aerodynamics. 2016 Mar 1;150:31-41.

22. He L, Hang J, Wang X, Lin B, Li X, Lan G. Numerical investigations of flow and passive pollutant exposure in high-rise deep street canyons with various street aspect ratios and viaduct settings. Science of the Total Environment. 2017 Apr 15;584:189-206.

23. Takano Y, Moonen P. On the influence of roof shape on flow and dispersion in an urban street canyon. Journal of Wind Engineering and Industrial Aerodynamics. 2013 Dec 1;123:107-20.

24. Ai ZT, Mak CM. CFD simulation of flow in a long street canyon under a perpendicular wind direction: Evaluation of three computational settings. Building and Environment. 2017 Mar 1;114:293-306.

25. Ghobadi P, Nasrollahi N. Assessment of pollutant dispersion in deep street canyons under different source positions: Numerical simulation. Urban Climate. 2021 Dec 1;40:101027.

26. Hang J, Chen X, Chen G, Chen T, Lin Y, Luo Z, Zhang X, Wang Q. The influence of aspect ratios and wall heating conditions on flow and passive pollutant exposure in 2D typical street canyons. Building and Environment. 2020 Jan 15;168:106536.

27. Zheng X, Yang J. CFD simulations of

wind flow and pollutant dispersion in a street canyon with traffic flow: Comparison between RANS and LES. Sustainable Cities and Society. 2021 Dec 1;75:103307.

28. Vardoulakis S, Fisher BE, Pericleous K, Gonzalez-Flesca N. Modelling air quality in street canyons: a review. Atmospheric environment. 2003 Jan 1;37(2):155-82.

29. Xie X, Huang Z, Wang JS. Impact of building configuration on air quality in street canyon. Atmospheric Environment. 2005 Aug 1;39(25):4519-30.

30. Huang Y, Hu X, Zeng N. Impact of wedge-shaped roofs on airflow and pollutant dispersion inside urban street canyons. Building and Environment. 2009 Dec 1;44(12):2335-47.

31. Kastner-Klein P, Plate EJ. Wind-tunnel study of concentration fields in street canyons. Atmospheric Environment. 1999 Oct 1;33(24-25):3973-9.

32. Baik JJ, Kwak KH, Park SB, Ryu YH. Effects of building roof greening on air quality in street canyons. Atmospheric Environment. 2012 Dec 1;61:48-55.

33. Tominaga Y, Mochida A, Yoshie R, Kataoka H, Nozu T, Yoshikawa M, Shirasawa T. AIJ guidelines for practical applications of CFD to pedestrian wind environment around buildings. Journal of wind engineering and industrial aerodynamics. 2008 Oct 1;96(10-11):1749-61.

34. Meroney RN, Pavageau M, Rafailidis S, Schatzmann M. Study of line source characteristics for 2-D physical modelling of pollutant dispersion in street canyons. Journal of wind Engineering and industrial Aerodynamics. 1996 Aug 1;62(1):37-56.

35. Xiaomin X, Zhen H, Jiasong W. The impact of urban street layout on local atmospheric environment. Building and Environment. 2006 Oct 1;41(10):1352-63.

36. Sini JF, Anquetin S, Mestayer PG. Pollutant dispersion and thermal effects in urban street canyons. Atmospheric environment. 1996 Aug 1;30(15):2659-77.

37. Jeong SJ, Andrews MJ. Application of the k–ε turbulence model to the high Reynolds number skimming flow field of an urban street canyon. Atmospheric environment. 2002 Mar 1;36(7):1137-45.